INFLUENCE OF MAINSTREAM REYNOLDS NUMBER AND MASS-FLOW RATIO ON THE FILM COOLING EFFICIENCY OF TURBINE BLADES

by

Lina ZHANG*, Kunpeng CAO, and Junfen LI

School of Aeronautical Engineering, Zhengzhou University of Aeronautics, Zhengzhou, China

Original scientific paper
https://doi.org/10.2298/TSCI2602179Z

It is imperative to implement advanced blade cooling technologies to ensure the seamless functioning of aeroengine turbine blades in high temperature environments. The mainstream flow is a pivotal factor influencing the film cooling efficiency of turbine blades. In this paper, the influence mechanism of the mainstream flow on the film cooling efficiency of turbine blades under different mainstream Reynolds numbers and mass-flow ratios is thoroughly investigated. The distribution laws of the cooling efficiency on the pressure surface and the suction surface, as well as the changes in the flow velocity of the central section of the blade, are elaborated in detail. The findings of the research indicate that when the mass-flow ratio is fixed, the cooling efficiency is higher under conditions of a lower mainstream Reynolds number. As the mass-flow ratio increases, the influence of the mainstream Reynolds number on the cooling efficiency gradually weakens. The cooling efficiency on the pressure surface experiences a decrease, while that on the suction surface initially decreases and subsequently increases. Furthermore, an increase in cold air-flow results in a greater accumulation of film in the middle-height region of the blade. This phenomenon enhances the cooling efficiency in this specific area. However, the enhancement of cooling efficiency along the upper and lower wall surfaces is not substantial.

Key words: *cooling efficiency, mainstream flow, mass-flow ratio, Reynolds number*

Introduction

The cooling characteristics of turbine blades are of paramount importance for the proper functioning of aeroengines [1, 2]. Among the numerous factors influencing the cooling efficiency of turbine blades, the mainstream flow is a critical one [3]. This phenomenon exerts a substantial influence on the distribution of cold air over the turbine blades and has the potential to induce local thermal deformation within the blade structure. This deformation can potentially result in blade damage, thereby affecting the performance and reliability of the aeroengine [4, 5].

On a global scale, studies concerning the impact of the mainstream Reynolds number on the film cooling efficiency of turbine blades have proven to be a highly active area of research. Van Fossen *et al.* [6] conducted an experimental exploration into the impact of mainstream Reynolds number and turbulent characteristics on the heat transfer at the blade

* Corresponding author, e-mail: lina810619@163.com

stagnation point. Ou *et al.* [7] conducted a comprehensive investigation into the impact of unsteady wakes on film cooling and heat transfer in turbine blades. Hylton *et al.* [8] investigated the influence of the mainstream Reynolds number on film cooling, with a particular emphasis on relatively high Reynolds numbers. Liu and Liu [9] conducted a wind tunnel experiment to investigate the heat transfer process of a turbine guide cascade film. Su *et al.* [10] investigated the internal cooling mechanisms of turbine moving blades and determined that the effect of blade heat conduction on the blade temperature field was highly significant. Wang *et al.* [11] conducted a measurement of the blade surface pressure distribution at inlet Reynolds numbers of 5×10^5, 6×10^5, and 7×10^5 in a wind tunnel. He then proceeded to calculate the heat transfer coefficient distribution on the blade surface for each inlet Reynolds number.

In recent years, foreign experimental research has mainly focused on constructing experimental databases and providing data support for improved numerical methods [12-16]. Li and Zhu [17, 18] explored control strategies for the aerodynamic stability of the cascade in heat transfer wind tunnels, as well as the experimental setups and heat transfer data processing methods for blade heat transfer measurements. Comprehensive pressure and heat transfer measurements of both the moving and stationary blade surfaces were conducted [19], and it was determined that the Reynolds number was the primary factor influencing heat transfer on the blade surfaces.

However, despite the significant progress made in previous studies, there is still a lack of a comprehensive understanding of the combined effects of the mainstream Reynolds number and mass-flow ratio (MFR) on the film cooling efficiency of turbine blades under various working conditions. In the present study, we aim to fill this gap by systematically scrutinizing the effect of the mainstream on the film cooling efficiency of the turbine blade under diverse Reynolds numbers and MFR. This research is expected to provide valuable insights and theoretical support for the design and optimization of aeroengine turbine blade cooling systems.

Computational model and boundary conditions

As illustrated in fig. 1, the diameter of the film cooling holes, d, measures 0.988 mm. The hole spacing, P, is 3.333 times d. The outflow direction of the film cooling hole forms a 45° angle with the wall surface in the radial direction. A total of 17 rows of film cooling holes are arranged on the blade. Each row contains 35 holes, with 3 rows on the suction surface of the leading edge, 4 rows on the pressure surface of the leading edge. The cooling air-flow emerging from the leading-edge film holes creates an opposing structure against the mainstream gas, which plays a crucial role in the heat transfer process. Additionally, there are 4 rows on the blade suction surface and 6 rows on the blade pressure surface. For the convenience of identification and analysis, the film cooling holes in the leading-edge section are labeled as L1-L7, those on the pressure surface of the blade are designated as P1-P6, and the ones on the suction surface of the blade are identified as S1-S4.

The boundary conditions are presented in fig. 1(b). The two sides of the computational domain are subjected to periodic boundary conditions, which simulate the repetitive nature of the blade cascade in a real-world scenario. The mainstream gas enters through the inlet, while the cooling air enters from above. The cooling air then exits from the film holes, effectively cooling the wall surface of the blade.

The computational model is partitioned into several key regions: the mainstream inlet, cold air inlet, outlet, and periodic boundaries on both sides. The height of both the inlet and outlet is set to 120 mm, and their length is 175 mm. In the middle section, the blade

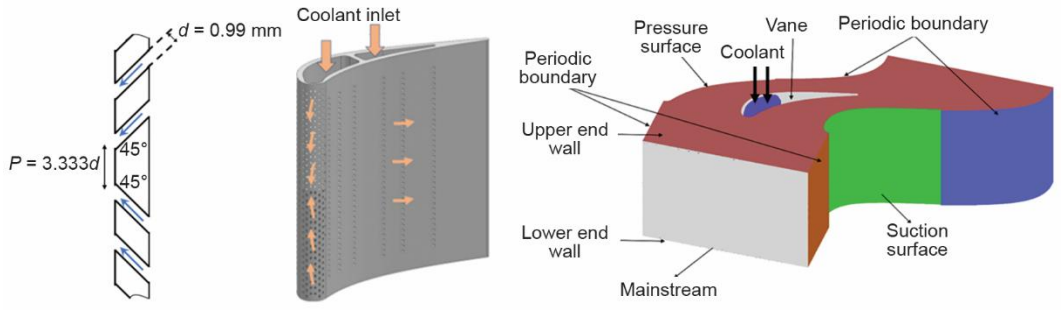

Figure 1. Schematic diagram of computational model; (a) blade film hole structure and (b) boundary condition

chord, *c*, is 121 mm, and the blade height, *h*, is 175 mm. The cascade passage, *W*, represents the middle flow-field section sandwiched between the pressure-surface boundary and the suction-surface boundary. This well-defined model structure and boundary conditions ensure the accuracy and reliability of the numerical simulations, enabling a more in-depth exploration of the complex flow and heat transfer phenomena within the turbine blade cooling system.

Grid distribution

The grid distribution and its local details are depicted in fig. 2. For the meshing process, a tetrahedral grid is selected as the fundamental grid type due to its flexibility in adapting to complex geometries. In the vicinity of the wall, where the flow characteristics are highly influenced by the no-slip condition and viscous effects, a prismatic grid is employed. This combination allows for a more accurate representation of the boundary-layer flow.

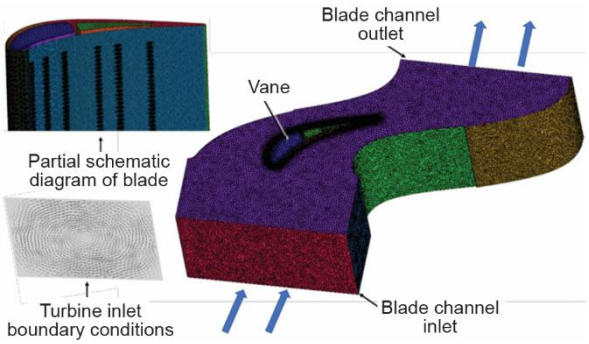

Figure 2. Schematic grids of calculation model

In the computational domain of the film cooling simulation section and the cascade test section, specific grid parameters are carefully determined. The height of the first grid layer is set to 0.5 and 0.001, respectively. The prismatic grids in these regions consist of 15 and 30 layers, with a growth rate of 1.2. This growth rate is chosen to balance the need for resolution near the wall and computational efficiency. A growth rate of 1.2 ensures that the grid cells gradually expand away from the wall, capturing the variation in flow properties effectively without excessive grid refinement in regions where it is not necessary.

After a comprehensive consideration of the trade-off between the number of grids, computational accuracy, and computational time, the optimal number of computing grids

adopted in this study is determined to be 15 million. This number is sufficient to provide accurate results while keeping the computational cost within a reasonable range.

The SST *k-ω* models with transition equations are chosen for computing the flow in the cascade passage. These models have demonstrated certain advantages in accurately calculating the flow structure within the cascade passage. They can effectively capture the complex interactions between the mainstream flow and the cooling air, as well as the boundary-layer transition phenomena.

The mainstream inlet is specified with a *velocity* boundary condition, which precisely defines the speed of the incoming mainstream gas. The outlet pressure is set to 101.325 kPa, representing the standard atmospheric pressure at the outlet. The coolant inlet is defined with a mass-flow boundary condition, enabling accurate control of the amount of cooling air entering the system. In the coolant inlet, the gas type is set as air, and the turbulence intensity is set at 2% to account for the inherent turbulence in the cooling air-flow. Table 1 displays the complete list of calculation parameters, providing a clear overview of all the variables used in the simulations.

Definition of parameters

The Reynolds number is defined as $\mathrm{Re} = \rho u d/\mu$, where u [ms^{-1}] represents the fluid velocity, ρ [kgm^{-3}] – the fluid density, d [m] – the vertical diameter of the fluid inlet channel, and μ [kgm^{-1}s^{-1}] – the fluid viscosity.

The MFR is the ratio of the cold air mass-flow to the incoming gas mass-flow. It is calculated as $MFR = q_{m1}/q_{m2}$, where q_{m1} is the mass-flow rate of the cold air and q_{m2} – the mass-flow rate of the mainstream gas. In this study, the MFR of 0.7, 1.0, and 1.3 are investigated. Notably, at the design point, the MFR for the leading edge cold air-flow is 7.09% and for the trailing edge cold air-flow is 1.77%.

The cooling efficiency, η, is a dimensionless parameter that characterizes the cooling effect. It is given by $\eta = (T - T_2)/30$, where T_1 [K] is the mainstream gas temperature, T_2 [K] – the surface temperature of the blade, and $\Delta T = 30$ [K] – the difference between the gas temperature and the cold air temperature. Table 1 presents the list of calculation parameters.

Table 1. List of calculation parameters

Main flow, Re	Gas velocity [ms^{-1}]	MFR	Leading edge q_{m1} [kgs^{-1}]	Leading edge q_{m2} [kgs^{-1}]
1×10^5	12.072	0.7	0.0154	0.00385
1×10^5	12.072	1.0	0.022	0.00550
1×10^5	12.072	1.3	0.0286	0.00715
3×10^5	36.209	0.7	0.0462	0.0115
3×10^5	36.209	1.0	0.0660	0.0165
3×10^5	36.209	1.3	0.0859	0.0214
5×10^5	60.347	0.7	0.0770	0.0192
5×10^5	60.347	1.0	0.110	0.0275
5×10^5	60.347	1.3	0.143	0.0357

Analysis of cooling characteristic

Figure 3 showcases the distribution of the blade film cooling efficiency on both the suction surface and the pressure surface under different MFR. When the MFR is 0.7, it is quite evident that the cooling efficiency on the suction surface is significantly higher than that on the pressure surface. As the MFR of the cold air increases, a distinct trend emerges: the cooling efficiency on the suction surface shows a decreasing tendency, while the cooling efficiency on the pressure surface exhibits an increasing one. When the MFR reaches 1.3, the cooling efficiencies on the suction and pressure surfaces start to converge.

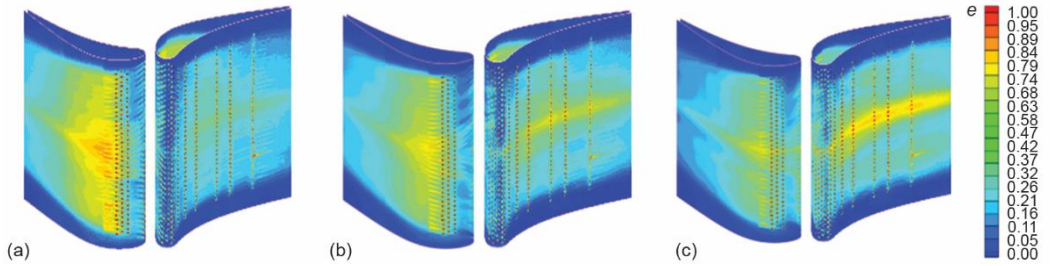

Figure 3. Distribution of film cooling efficiency under different MFR; (a) MFR = 0.7, (b) MFR = 1.0, and (c) MFR = 1.3

Generally, the area in the vicinity of the film holes features a relatively high cooling efficiency, which gradually declines in the downstream direction. Although only three rows of film holes are arranged on the suction surface, the cold air expands remarkably well towards the downstream. As a result, the entire suction surface is effectively covered by an air film, contributing to its relatively high cooling efficiency. In the region near the end wall, however, the cooling efficiency drops to zero. This can be attributed to two main factors. Firstly, there are no cooling film holes in these areas, leaving no direct source of cold air for cooling. Secondly, the presence of channel vortices near the end wall plays a role. The rotation of these vortices disrupts the spread of cold air towards the end wall, preventing effective cooling in this region.

Figures 4-6, respectively, illustrate the distributions of cooling efficiency at various Reynolds numbers on the pressure surface for MFR of 0.7, 1.0, and 1.3. By closely observing these diagrams, it becomes clear that along the height direction of the turbine blade, due to the dense arrangement of the leading-edge film holes, the mainstream gas and the cold air form an opposing configuration. This unique arrangement leads to a relatively higher cooling efficiency in the middle section of the blade.

At lower Reynolds numbers, an increase in the cold air-flow rate causes more air films to converge towards the higher region of the blade. This convergence effectively enhances the cooling efficiency in that area. However, the improvement in cooling efficiency near the upper and lower end walls is not particularly significant. Notably, the middle region of the blade is the key area with high cooling demands. Therefore, this distribution pattern of film cooling efficiency is well-aligned with the cooling requirements of turbine guide vanes.

At lower MFR, a significant difference in the leading-edge cooling efficiency can be observed between Reynolds numbers of 100000 and 300000. As the Reynolds number increases, the variation in cooling efficiency becomes less prominent. Additionally, as the MFR rises, the influence of the mainstream Reynolds number on the blade cooling efficiency gradually weakens.

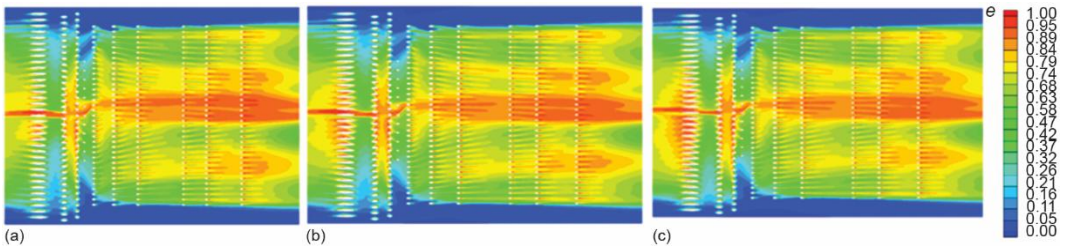

Figure 4. Distribution of cooling efficiency at MFR = 0.7; (a) Re = 1×10^5, (b) Re = 3×10^5, and (c) Re = 5×10^5

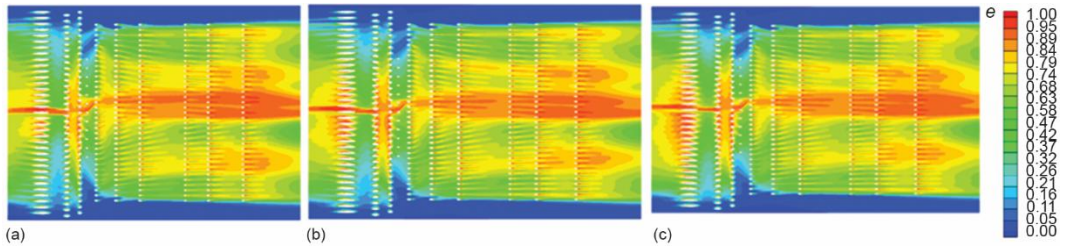

Figure 5. Distribution of cooling efficiency at MFR = 1.0; (a) Re = 1×10^5, (b) Re = 3×10^5, and (c) Re = 5×10^5

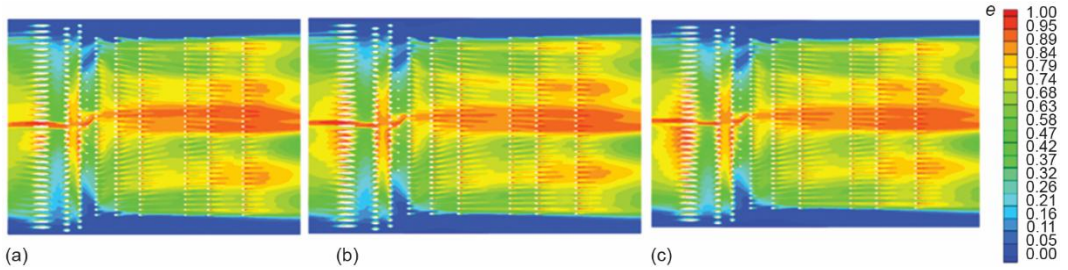

Figure 6. Distribution of cooling efficiency at MFR = 1.3; (a) Re = 1×10^5, (b) Re = 3×10^5, and (c) Re = 5×10^5

Figure 7 presents the area-averaged cooling efficiency values of the pressure surfaces at different Reynolds numbers for MFR values of 0.7, 1.0, and 1.3. From these graphs, it can be clearly seen that each peak corresponds to the location of the air-film holes. As the distance from the air-film holes increases, the cooling efficiency decreases. Under a fixed MFR, the cooling efficiency is relatively higher at lower mainstream Reynolds numbers. As the mainstream Reynolds number increases, the impact of the Reynolds number on the cooling efficiency becomes less substantial. Moreover, as the MFR increases, the influence of the mainstream Reynolds number on the cooling efficiency further weakens.

At lower MFR, the cooling air adheres better to the blade wall, which is beneficial for a higher leading-edge efficiency. However, at the trailing edge, due to the stronger carrying effect of the mainstream gas, the cooling efficiency of the cold air on the wall decreases. Compared with higher MFR, the cooling efficiency drops considerably.

Figure 8 shows the distributions of the total cooling efficiency in relation to the Reynolds number under different MFR. It can be observed that for the pressure surface, at

MFR values of 0.7 and 1.0, an increase in the mainstream Reynolds number has a significant impact on the total cooling efficiency. However, when the MFR is 1.3, the change in the mainstream Reynolds number has a less pronounced effect on the total cooling efficiency.

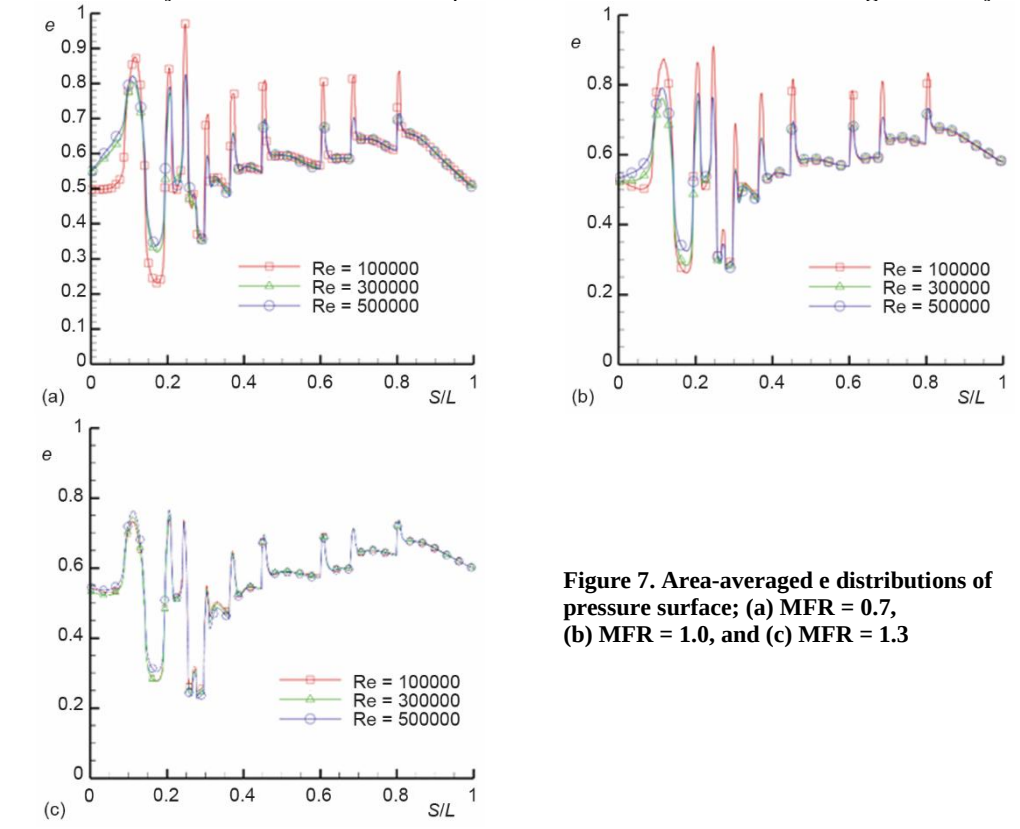

Figure 7. Area-averaged e distributions of pressure surface; (a) MFR = 0.7, (b) MFR = 1.0, and (c) MFR = 1.3

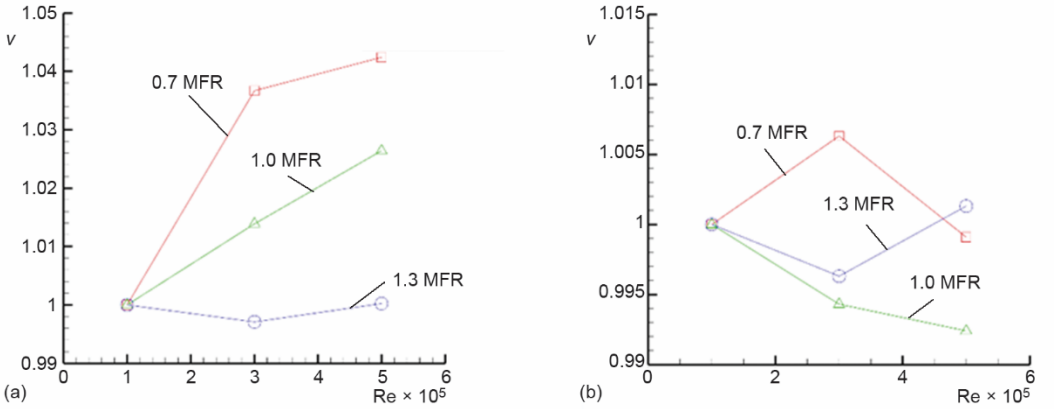

Figure 8. The total cooling efficiency distributions with Reynolds number; (a) pressure surface and (b) suction surface

Regarding the suction surface, at an MFR of 0.7, the total cooling efficiency initially increases and then decreases as the Reynolds number rises, which has a significant influence on the overall cooling performance. When the MFR is 1.0, as the mainstream Reynolds number increases, the overall cooling efficiency decreases. In the case of an MFR of 1.3 and at high flow rates, as the mainstream Reynolds number increases, the total cooling efficiency first decreases and then increases. As the MFR increases, the cooling efficiency on the pressure surface decreases, while the cooling efficiency on the suction surface first decreases and then increases.

Taking the case where the Reynolds number is 100000 and the MFR is 0.7 as an example, when the Reynolds number is set to 300000 and 500000, the total cooling efficiency on the pressure surface experiences an increase of 3.67% and 4.24%, respectively. At the same time, on the suction surface, it increases by 0.63% when the Reynolds number is 300000, whereas it decreases by 0.09% when the Reynolds number is 500000.

When the MFR is 1.0, the total cooling efficiency on the pressure surface shows an increment of 1.39% and 2.64%, respectively, for Reynolds numbers of 300000 and 500000. In contrast, on the suction surface, the total cooling efficiency decreases by 0.57% and 0.76%, respectively, for the same Reynolds numbers.

For an MFR of 1.3, on the pressure surface, the total cooling efficiency decreases by 0.29% compared to the case when the Reynolds number is 300000 and increases by 0.02% when compared to the situation where the Reynolds number is 500000. On the suction surface, it decreases by 0.37% relative to the case with a Reynolds number of 300000 and increases by 0.13% in relation to the scenario where the Reynolds number is 500000. This detailed analysis of the cooling characteristics provides a comprehensive understanding of how different parameters affect the film cooling efficiency of turbine blades, which is crucial for optimizing the design and performance of turbine cooling systems.

Analysis of flow characteristics

Figures 9-11, respectively, illustrate the velocity distribution within the middle section of the turbine blade under diverse MFR when Re is set to 100000, 300000, and 500000. These figures vividly demonstrate that as the mainstream Reynolds number varies, the mainstream gas and cooling air interact and mix on the blade surface, giving rise to distinct flow characteristics.

Due to the inherent nature of the internal flow, the pressure at the leading edge of the blade reaches its maximum value. This is because the mainstream gas converges at the leading edge before flowing around the blade. As the flow progresses downstream, the pressure gradually diminishes. Notably, within the scope of this study, there is no discernible radial pressure gradient, which simplifies the analysis of the flow field to a certain extent.

In fig. 9, when Re = 100000, the pressure from the leading edge to the suction surface exhibits a unique trend. Initially, the pressure rises as the flow moves from the leading edge towards the suction surface. However, it subsequently declines. This is closely related to the velocity distribution. At the trailing edge of the blade suction surface, the velocity is nearly zero. As a result, the pressure gradient within the cascade channel undergoes a transition from a clockwise gradient to a counterclockwise gradient. This change in the pressure gradient is the root cause of the initial increase and subsequent decrease in velocity.

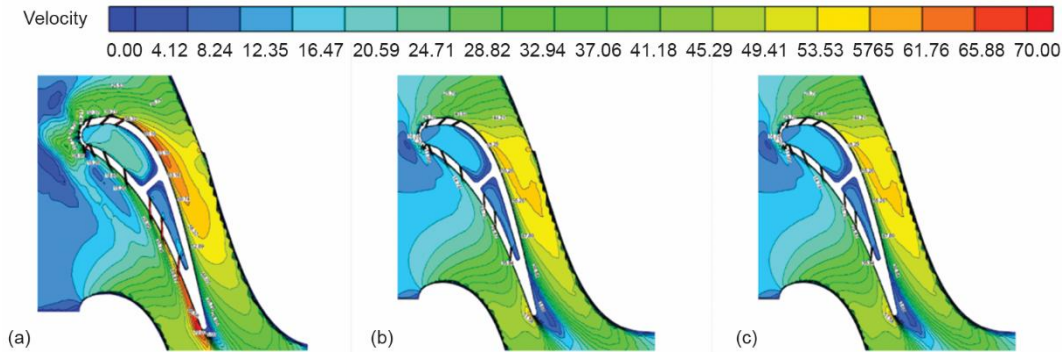

Figure 9. Velocity distribution under different MFR when Re = 100000; (a) MFR = 0.7, (b) MFR = 1.0, and (c) MFR = 1.3

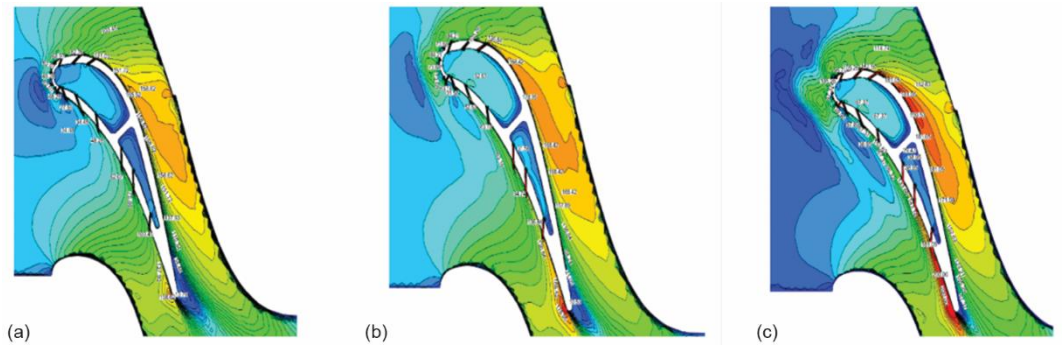

Figure 10. Velocity distribution under different MFR when Re = 300000; (a) MFR = 0.7, (b) MFR = 1.0, and (c) MFR = 1.3

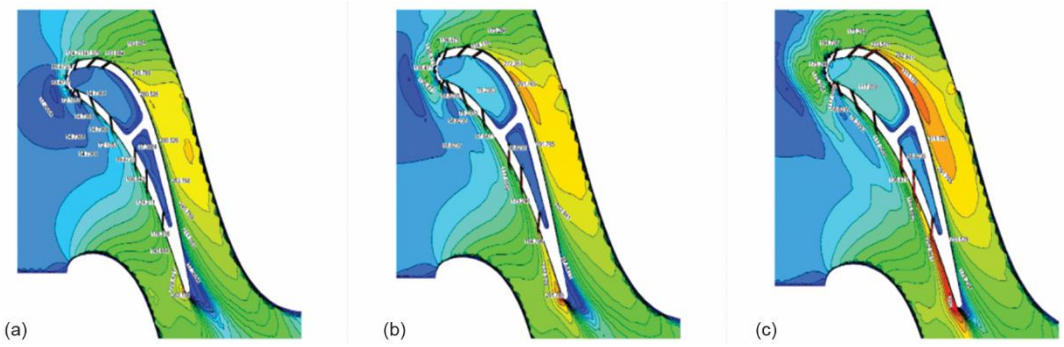

Figure 11. Velocity distribution under different MFR when Re = 500000; (a) MFR = 0.7, (b) MFR = 1.0, and (c) MFR = 1.3

By comparing the three different MFR, an interesting phenomenon can be observed. As the MFR increases, the area of the reverse pressure gradient decreases. This reduction in the reverse pressure gradient area is beneficial as it ameliorates the low speed zone in the wake of the suction surface. In other words, it alleviates the severe issue of mixing between the cold air and the mainstream gas. On the pressure surface of the blade, the velocity of the

mainstream gas shows an increasing tendency. However, the air film holes on the leading-edge pressure surface are directly exposed to the impact of the mainstream gas. Consequently, in this region, the mainstream gas and the cooling air-flow experience intense mixing. This mixing leads to a significant loss in velocity and an elevation in the temperature of the leading-edge blades. Fortunately, as the MFR escalates, the cooling air-flow adheres more effectively to the blade surface, which helps to mitigate the negative effects of this mixing to some degree.

From figs. 10 and 11, it becomes evident that as the MFR continues to increase, the area of the reverse pressure gradient on the suction surface progressively shrinks. This shrinkage effectively mitigates the air-flow mixing phenomenon induced by the reverse pressure gradient. In the rear portion of the suction surface, as the MFR rises, the high speed area gradually migrates away from the wall. This movement of the high speed area can have a profound impact on the heat transfer and cooling efficiency in this region.

On the leading-edge pressure surface, as the MFR increases, the cooling air-flow and the mainstream gas are arranged in an opposing manner. The intense mixing of the cold air and the mainstream gas at the leading edge generates conspicuous vortices. These vortices exacerbate the air-flow mixing, which may potentially lead to a decline in the cooling efficiency of the blade leading edge. This highlights the complex and delicate balance between the MFR, flow mixing, and cooling efficiency.

When comparing the alterations in the velocity field of the middle section under different mainstream Reynolds numbers while maintaining the same MFR, it is found that as the mainstream Reynolds number increases, the velocity of the suction surface correspondingly rises. This increase in velocity effectively enhances the reverse pressure gradient of the suction surface. Simultaneously, the velocity gradient on the pressure surface also augments with the growth of the mainstream Reynolds number. Overall, the velocity of the suction surface is greater than that of the pressure surface. Moreover, as the cold air-flow rate increases, the changes in the low speed field at the trailing edge are ameliorated. This improvement mitigates the mixing phenomenon between the mainstream gas and the cooling air-flow and ultimately enhances the efficiency of film cooling. This comprehensive analysis of the flow characteristics provides valuable insights into the complex fluid-flow mechanisms within the turbine blade, which is essential for optimizing the design and performance of turbine cooling systems.

Conclusions

This study systematically investigated the impact of the mainstream flow Reynolds number and the MFR on the film cooling efficiency of turbine blades, elucidating the intricate influence mechanism of the mainstream flow on the film cooling characteristics. The principal findings are summarized as follows.

When the MFR remains constant, a lower mainstream Reynolds number results in a higher cooling efficiency. As the mainstream Reynolds number increases, its influence on determining the cooling efficiency gradually weakens. Furthermore, as the MFR increases, the impact of the mainstream Reynolds number on cooling efficiency becomes less significant. This suggests that at lower Reynolds numbers, the interaction between the mainstream and the cooling air is more conducive to heat transfer and cooling. Conversely, higher MFR tend to reduce the sensitivity of the cooling efficiency to changes in the Reynolds number.

From the perspective of the turbine blade height direction, the dense arrangement of air film holes at the leading edge leads to an opposing configuration between the mainstream

gas and the cold air. This configuration results in a comparatively enhanced cooling efficiency within the medial segment of the blade. As the Reynolds number increases at lower MFR, the convergence of air films toward the middle-height region of the blade is augmented by the increase in cold air-flow rate. This convergence effectively enhances the cooling efficiency in this area. However, the enhancement in cooling efficiency along the upper and lower end walls is not significant. This phenomenon is likely attributable to the intricate flow patterns and the impact of secondary flows in proximity to the end walls. In general, the middle-height blade area is the key region with high cooling demands, and the distribution pattern of the film cooling efficiency aligns well with the cooling requirements of turbine guide vanes. This finding provides significant guidance for the design and optimization of turbine blade cooling structures, suggesting that greater attention should be directed towards enhancing the cooling effect in the middle-height region.

In summary, it is imperative to comprehend these relationships to ensure the optimal design of film cooling for turbine blades. Subsequent research endeavors could concentrate on delving deeper into the collective impact of various factors, including but not limited to distinct blade geometries, cooling hole configurations, and surface roughness, on the efficacy of film cooling. In addition, experimental verification of the numerical results presented in this study would enhance the reliability and practical application of the findings. This research not only deepens our understanding of the film cooling process but also offers valuable theoretical support for improving the performance and durability of aeroengine turbine blades.

Acknowledgment

This research was funded by the training program for young key teachers of Henan Higher Education Institutions, grant number 2019GGJS180, the Henan Province Science and Technology Research Project, grant number 242102240053, 242102240049.

References

[1] Long, T. Y., *et al.*, Wind Turbine Blades with Hybrid Fiber Composite Tensile Properties and Numerical Verification, *Thermal Science*, *28* (2024), 3A, pp. 2109-2114
[2] Soori, M., Asmael, M., Minimization of Deflection Error in Five Axis Milling of Impeller Blades, *Facta Universitatis – Series Mechanical Engineering*, *21* (2023), 2, pp. 175-190
[3] Wang, K., *et al.*, Impact of V-Shaped Interrupted Ribs in Cross-Flow Channels on Film Cooling, *Thermal Science*, *28* (2024), 4A, pp. 3093-3106
[4] Nourin, F. N., Amano, R. S., Review of Gas Turbine Internal Cooling Improvement Technology, *Journal of Energy Resources Technology*, *143* (2021), 080801-1
[5] He, Q. Z., *et al.*, Research on Cooling Structure Design of High Pressure Turbine Blade for Intercooled Gasturbine, *Journal of Engineering for Thermal Energy and Power*, *35* (2020), 7, pp. 28-34
[6] Van Fossen, G. J., *et al.*, Influence of Turbulence Parameters, Reynolds Number, and Body Shape on Stagnation Region Heat Transfer, *Heat Transfer, 117* (1995), 3, pp. 597-603
[7] Ou, S., *et al.*, Unsteady Wake on a Linear Turbine Blade Cascade with Air and CO_2 Film Injection: Part 1-Effect on Heat Transfer Coefficients, *Journal of Turbine Machinery, 116* (1994), pp. 721-729
[8] Hylton, L. D., *et al.*, Analytical and Experiment Evaluation of the Heat Transfer Distribution over the Surface of Turbine Vane, Report NASA-CR-168015, NASA, 1985
[9] Liu, G. W., Liu, S. L., Influence of Injection Angle on the Aerodynamic Aspects of Endwall Film-Cooling in a Turbine Cascade, *Journal of Propulsion Technology*, *25* (2004), 3, pp. 206-209
[10] Su, S., *et al.*, Numerical Simulation of Conjugate Heat Transfer for an Internally Cooled 3-D Turbine Blade, *Journal of Aerospace Power*, *22* (2007), 12, pp. 2018-2024
[11] Wang, Y. D., *et al.*, Effects of Reynolds Number and Turbulence Intensity on Boundary Layer Transition and Heat Transfer Characteristics of Blade Surface, *Science Technology and Engineering*, *21* (2021), 33, pp. 14415-14421

[12] Abu-Gharmam, B. J., Shaw, R., Natural Transition of Boundary Layers the Effects of Turbulence, Pressure Gradient, and Flow History, *Journal of Mechanical Engineering Science*, *22* (1980), 5, pp. 213-228
[13] Giel, P. W., *et al.*, Measurements and Predictions of Heat Transfer on Rotor Blades in a Transonic Turbine Cascade, *Journal of Turbomachinery*, *126* (2004), 1, pp. 110-121
[14] Haldeman, C. W., *et al.*, Aerodynamic and Heat-Flux Measurements with Predictions on a Modern One and One Half State High Pressure Transonic Turbine, *Journal of Turbomachinery,127* (2005), 3, pp. 522-531
[15] Tallman, J. A., *et al.*, Heat Transfer Measurements and Predictions for a Modern, High-Pressure, Transonic Turbine, Including Endwalls, *Journal of Turbomachinery*, *131* (2009), 2, pp. 1-14
[16] Kays, W. M., *et al.*, *Convective Heat and Mass Transfer*, 4th ed., McGraw-Hill, New York, USA, 2005
[17] Li, H. C., Zhu, H. R., Aerodynamic State Regulation and Control of Cascade in Short Duration Wind Tunnel, *Advances in Areonautical Science and Engineering*, *4* (2013), 4, pp. 463-468
[18] Li, H. C., Zhu, H. R., Cascade Heat Transfer Experiment Validation in Short Duration Transonic Wind Tunnel, *Journal of Xi An Jiao Tong University*, 47 (2013), 9, pp. 49-54
[19] Fu, Z. Y., *et al.*, Experimental Study of Full Coverage Film Cooling Effectiveness of Turbine Guide Vane with W-Shaped Holes, *Journal of Propulsion Technology*, *42* (2021), 9, pp. 2028-2037

Paper submitted: December 4, 2024
Paper revised: May 5, 2025
Paper accepted: May 13, 2025
2026 Published by the Vinča Institute of Nuclear Sciences, Belgrade, Serbia.
This is an open access article distributed under the CC BY-NC-ND 4.0 terms and conditions.